A Novel Human Extravascular Monocyte Subset with Antiviral Functions Is Crucial for Resolving Lung Tissue Infection

Devin Kenney, Aoife O'connell, Anna Tseng, Jacquelyn Turcinovic, Maegan Sheehan, Adam Nitido, Paige Montanaro, Hans Gertje, Maria Ericsson, John Connor, et al.

Title: A Novel Human Extravascular Monocyte Subset with Antiviral Functions Is Crucial for Resolving Lung Tissue Infection

Short Title: Extravascular Monocytes Resolve Lung Infection

One sentence summary: We identified a novel human subset of lung extravascular monocytes with antiviral functions that play a critical role in resolving SARS-CoV-2 infection from human lung tissues in an immunologically naïve context.

Devin Kenney[1,2], Aoife K. O'Connell[1,2,4], Anna E. Tseng[1,2,4], Jacquelyn Turcinovic[1,2,3], Maegan L. Sheehan[7,12], Adam D. Nitido[7,12], Paige Montanaro[2,4], Hans P. Gertje[2,4], Maria Ericsson[6], John H. Connor[1,2], Vladimir Vrbanac[7], Nicholas A. Crossland[1,2,4], Christelle Harly[8,9,12]*, Alejandro B. Balazs[7,12]*, and Florian Douam[1,2,12,13]*

[1]Department of Virology, Immunology, and Microbiology, Boston University Chobanian & Avedisian School of Medicine, Boston, MA, USA.

[2] National Emerging Infectious Diseases Laboratories, Boston University, Boston, MA, USA.

[3] Bioinformatics Program, Boston University, Boston, MA, USA.

[4] Department of Pathology and Laboratory Medicine, Boston University Chobanian & Avedisian School of Medicine, Boston, MA, USA.

[6] Electron Microscopy Core Facility, Harvard Medical School, Boston, MA, USA.

[7] Ragon Institute of MGH, MIT and Harvard, Cambridge, MA, USA.

[8] Université de Nantes, INSERM, CNRS, CRCINA, Nantes, France

[9] LabEx IGO 'Immunotherapy, Graft, Oncology', Nantes, France.

[12] These authors contributed equally to the work.

[13] Lead contact

*Correspondence:

Florian Douam, National Emerging Infectious Diseases Laboratories, 620 Albany Street Boston MA 02118 USA, +1-617-358-9174, fdouam@bu.edu.

Alejandro B. Balazs, Ragon Institute of MGH Harvard and MIT, 400 Technology Square Cambridge MA 02139 USA, +1-857-268-7197, abalazs@mgh.harvard.edu.

Christelle Harly, CRCINA - Institut de Recherche en Santé de Nantes Université, 8 quai Moncousu 44 007 Nantes France, +33-2 28 08 02 08, christelle.harly@inserm.fr.

The authors have declared that no conflict of interest exists.

ABSTRACT

The recurring emergence of novel respiratory viruses has highlighted our poor understanding of the human immune mechanisms governing the resolution of lung infection in an immunologically naïve context. Using SARS-CoV-2 as a prototypical emerging respiratory virus, we leveraged mice co-engrafted with a genetically matched fetal lung xenograft (fLX) and a human immune system (BLT-L mice) to investigate such mechanisms. While BLT-L mice effectively resolve SARS-CoV-2 infection following acute viral replication in fLX, viral clearance is robustly abrogated through systemic depletion of CD4+, but not CD3+ or CD8+ cells, resulting in persistent infection. Leveraging single-cell transcriptomics to uncover the CD4-expressing subsets driving infection resolution, we identified a novel subset of lung extravascular inflammatory monocytes (ExiMO) with antiviral functions. ExiMO are the dominant CD163-expressing myeloid population emerging in fLX upon acute infection and derive from recruited circulating CD4+ monocytes. They are highly enriched in viral RNA and elicit a robust antiviral response before vanishing from tissues when infection resolves. Notably, systemic CD4+ cell depletion results in impaired recruitment of CD163+ cells into fLX and leads to a state of immune tolerance and chronic infection defined by the absence of ExiMO antiviral responses. Together, our study uncovers ExiMO as major sentinels driving SARS-CoV-2 infection resolution in human lung tissues without pre-existing immunity. This work expands our understanding of lung extravascular monocytes and unravels novel facets of the cellular determinants governing our vulnerability to viral respiratory pathogens.

INTRODUCTION

Human emerging respiratory viruses (hERVs), including MERS-CoV, new influenza A strains, and more recently, SARS-CoV-2, the etiologic agent of COVID-19, have reignited the need to understand immunological mechanisms that can protect us against these pathogens when no pre-existing and/or cross-reactivity immunity exists. While these non-experienced immune mechanisms harbor a pivotal role in our inherent resistance against antigenically novel hERVs and their disruptive impact on public health, the scarcity of experimental systems that recapitulate lung-resident human immune responses has made their investigation challenging.

Human studies are associated with logistical and experimental challenges, such as the need to capture early pulmonary immune responses in infected individuals and/or in the validation of purely correlative findings. While these challenges can be overcome through experimental human infection studies, longitudinal lung-resident immune responses in infected volunteers remain hardly accessible. Notably, a recent human challenge study uncovered novel immunological signatures of protection from SARS-CoV-2 in humans (*1*). However, sample analysis was limited to peripheral blood and nasopharyngeal swabs, concealing major tissue-resident immunological processes associated with protection, such as extravasation of recruited immune lineages and their differentiation process to combat and resolve infection.

In contrast, large and small animal models have been developed to support infection with hERVs. However, the high cost and limited reagent availability associated with non-human primate models and the large divergence between rodent and human immune systems underscore the need for additional models capable of recapitulating human protective immune responses to HERVs in an immunologically non-experienced context.

Mice co-engrafted with human fetal lung xenograft (fLX) and a human immune system (HIS) have been reported to support infection by multiple hERVs, including human cytomegalovirus (HCMV), Middle East respiratory syndrome coronavirus (MERS-CoV) and SARS-CoV-2 (*2*-*4*), and mount lung-resident human immune responses against these pathogens.

Recently, our group reported that mice engrafted with fLX are highly susceptible to SARS-CoV-2 infection and lung tissue damage and support persistent viral infection. However, co-engraftment of these animals with fLX and a HIS in a xenorecipient strain supporting enhanced myelopoiesis (i.e., HNFL mouse model) prevented any detectable viral replication in fLX, resulting in complete lung tissue protection from histopathology (*3*). Our findings unraveled a human macrophage antiviral signature as a correlate of non-experienced immunity against SARS-CoV-2 infection. However, the non-experienced immune mechanisms governing the resolution of SARS-CoV-2 infection in the context of extensive viral replication in lung tissues, which more likely describes mild cases of COVID-19, have remained elusive. This study, which uses SARS-CoV-2 as a prototypical hERV, aims to unravel some of these mechanisms.

Unlike the HNFL mouse model, immunodeficient mice co-engrafted with fLX and a genetically matched human immune system, fetal liver, and thymus (BLT-L mice) support acute SARS-CoV-2 infection, consistent with previous reports (*2, 4*). However, the infection quickly resolves following a viral replication peak at 2 days post-inoculation (dpi), making this model suitable for examining mechanisms of non-experienced antiviral immunity in the context of HERV infection of lung tissues. Notably, systemic depletion of CD4+ cells, but not CD3+ T-cells or CD8+ cells, robustly abrogates infection resolution and results in persistent viral replication in fLX of BLT-L mice. Using single-cell transcriptomic and multiplexed immunohistochemistry (mIHC) approaches, we uncovered a novel subset of lung extravascular inflammatory monocytes (ExiMO). ExiMO are directly related to intravascular CD4+ patrolling monocytes recruited into fLX during acute infection, and are the dominant CD163-expressing myeloid subset to emerge in fLX upon acute infection. They are highly enriched in viral RNA and elicit a uniquely robust antiviral response. In accordance with our depletion findings, CD4+ cell depletion reduces CD163+ recruitment into fLX and promotes a state of immune tolerance characterized by the absence of major antiviral cytokines expressed by ExiMO. CD4+ cell depletion also induces systemic and lung signatures of chronic infection, underlining how ExiMO are critical to avert long-lasting viral

persistence. Collectively, our work sheds light on a novel cellular mediator driving naïve immunity against SARS-CoV-2 in human lung tissues. To our knowledge, our study is the first to uncover lung extravascular monocytes with antiviral functions and contributes to enhancing our understanding of the cellular determinants defining human susceptibility to hERVs.

RESULTS

BLT-L mice effectively clear SARS-CoV-2 infection following acute viral replication

Previous work from our laboratory (*3*) and others (*2, 4, 5*) have shown that immunodeficient mice can successfully be engrafted with human fetal lung xenograft (fLX) alone or in combination with a human immune system (HIS). In this study, we leveraged a previously reported mouse model co-engrafted with fetal liver and thymus as well as with human hematopoietic stem cells (HSC) and fLX (BLT-L mice) (*5*). Fetal liver and thymus were engrafted under the renal capsule of adult NOD.Cg-*Prkdc*^{scid} *Il2rg*^{tm1Wjl}/SzJ (NSG) mice (12-16 weeks old) prior to intravenous HSC injection. A piece of fetal lung tissue was subcutaneously engrafted on the flank of each animal, as described previously (*5*). To determine the susceptibility of BLT-L mice to SARS-CoV-2 infection and their ability to effectively clear infection, BLT-L mice were inoculated with SARS-CoV-2 (2019-nCoV/USA_WA1/2020) via intra-graft injection. We used a viral dose (10^6 PFU) that we previously established to drive robust and persistent infection in fLX of immunodeficient mice not engrafted with an HIS (*3*).

Throughout the course of infection, mice did not display any weight loss (**Fig. 1A)** or clinical signs of disease such as lethargy or lack of responsiveness (data not shown). To assess lung histopathology and viral titers longitudinally, fLX were collected at 2, 6, and 12 dpi. Immunohistochemistry (IHC) for SARS-CoV-2 Spike (S) protein revealed infection of alveolar epithelium in fLX at 2 dpi, while the majority of viral antigen was cleared by 6 dpi and became undetectable by 12 dpi (**Fig.1B**$^{a\text{-}d}$). SARS-CoV-2 S was primarily detected in the cytoplasm of alveolar epithelium morphologically consistent with type II pneumocytes (AT2 cells) and

157 macrophages within alveolar spaces admixed with necrotic cellular debris and bronchiole
158 epithelium, consistent with the primary cell targets of SARS-CoV-2 (**Fig.1B[b]**). These findings were
159 independently confirmed through IHC for SARS-CoV-2 nucleoprotein N (**Fig. S1A-D**).
160 Transmission electron microscopy (TEM) imaging of fLX at 2 dpi substantiated evidence of
161 productive fLX infection, as indicated by the presence of viral particles in the cytosol of epithelial
162 cells and budding/invagination of virions (**Fig. S1E-G**). Viral titer quantification in fLX also
163 supported evidence of acute infection at 2 dpi prior to effective resolution (**Fig.1C**). A significant
164 amount of infectious viral particles could be recovered from fLX at 2 dpi (3.20 ± 2.52 log([PFU/mg
165 of tissue]), but not at 6 dpi (0.281 ± 0.688 log[PFU/mg of tissue]) and 12 dpi (0.111 ± 0.293
166 log[PFU/mg of tissue]) (**Fig. 1C**).

167 Next, we examined histopathological phenotypes associated with active and resolved
168 infection. Interpretation of hematoxylin and eosin (H&E) staining illustrated denuding of
169 pneumocytes, neutrophil infiltration, edema, hemorrhage, thrombosis, and pneumocyte necrosis,
170 which correlated with sites of infection at 2 dpi (**Fig. 1B[e,f] and Fig. S1H-J**). No major disease
171 phenotypes were observed at 6 and 12 dpi compared to naïve fLX, underscoring that fLX can
172 mount repair mechanisms upon resolution of infection (**Fig. 1B[g,h]**). A previously described semi-
173 quantitative histopathological scoring system (*3*) provided statistical confirmation for a significant
174 increase in lung pathology at 2 dpi, which was no longer apparent at 6 dpi (**Fig. 1D**) or 12 dpi. Of
175 note, minor lung pathology was observed at baseline (naïve), likely reflecting limited graft vs. host
176 disease. Together, BLT-L fLX recapitulates important hallmarks of acute SARS-CoV-2 infection,
177 including viral replication and histopathological manifestations of disease, prior to effective viral
178 clearance and lung tissue repair.

179

180 **Humoral responses do not drive SARS-CoV-2 clearance in BLT-L mice despite evidence of**
181 **Spike selective pressure.**

We first asked whether SARS-CoV-2 infection resolution was driven by human neutralizing humoral responses. No neutralization against infectious SARS-CoV-2 was detected from the serum of BLT-L mice collected at 2 or 12 dpi (**Fig. S1K,L**). This is consistent with the rapid clearance of infectious viral particles by 6 dpi, and the known caveat that humanized mice mount limited humoral responses (*6*). However, viral genome sequencing from acutely infected fLX showed that 75% of 2 dpi-associated viral sequences exhibited the selection of two stable mutations not observed in our inoculum and located in the Spike N-terminal domain (NTD): an insertion (216KLRS) and a non-synonymous mutation (R245H) (**Fig. S1M,N Table S1**). Interestingly, these two mutations were found together in 100% of the viral sequences, suggesting potential co-evolution (**Fig. S1O**). They have also been reported as positively selected in the context of sub-optimal neutralizing antibody concentration (216KLRS) (*7*) or in the context of cross-species adaptation (216KLRS and R245H) (*8*). Despite the lack of humoral responses, these findings underscore how BLT-L mice can recapitulate host-pathogen interactions that drive SARS-CoV-2 evolution and host adaptation.

Systemic depletion of CD4+ cells abrogates viral clearance in fLX.

The addition of a human thymus in the BLT-L model generates a more functional T lymphocyte compartment. Therefore, we wished to examine the contribution of T cells in SARS-CoV-2 infection resolution. We performed systemic depletion of CD3+, CD4+, and CD8+ cells through the administration of OKT3, OKT4, or OKT8 depleting antibodies, respectively, via intraperitoneal injection both prior to and after infection (**Fig. 2A**). Effective systemic depletion was confirmed in the blood by flow cytometry (**Fig. S2A**). All animals were euthanized at 12 dpi to assess for the persistence of SARS-CoV-2 infection in fLX. While depletion of CD3+, CD4+, and CD8+ cells induced persistent infection in some or most of the animals, only CD4+ cell depletion (mean Log PFU/mg tissue = 2.37) resulted in a statistically significant defect in infection resolution compared to all other experimental conditions (isotype, OKT3, and OKT8-treated mice)

(**Fig. 2B**). The rate of productively infected fLX was also higher in CD4+ cell-depleted animals, with 72% of fLX (8/11) showing infection at 12 dpi compared to 50% (4/8) and 33% (2/6) in CD3- and CD8-depleted mice, respectively (**Fig. 2B**). Additionally, when examining the average viral titer (Log PFU/mg of tissue) of persistently infected fLX, the ones from CD4+ cell-depleted animals were significantly higher compared to CD3+ cell- depleted fLX (**Fig. S2B**), furthering that CD4+ cells have a more consequential impact on driving infection resolution than CD3+ cells. Anti-SARS-CoV-2 N IHC confirmed these findings and superior defect of CD4+ cell-depleted animals to resolve infection (**Fig. 2C**). Using multiplex fluorescent IHC (mIHC), we also validated the reduction in CD3+, CD4+ and CD3+ CD4- cells in fLX from CD3-, CD4- and CD8-depleted animals respectively, compared to isotype-treated animals (**Fig.2D**).

Persistent infection in CD4+ cell-depleted animals was also associated with significant downregulation of MHC class I (**Fig. 2E**), a phenomenon we similarly observed in acutely infected fLX (2 dpi) (**Fig. 2E**) and that has been previously reported in cells with active SARS-CoV-2 replication (*9, 10*). This further emphasizes that depletion of CD4+ cells is associated with defective viral clearance mechanisms. These findings suggest that circulating CD4-expressing cells, and to a lesser extent CD3+ T-cells, mediate SARS-CoV-2 infection resolution in BLT-L mice.

Human responses to SARS-CoV-2 mobilize specific hematopoietic subsets.

To define the identity of the CD4+, and to a lesser extent, CD3+ subset(s) mediating infection resolution, we performed single-cell RNA sequencing (scRNA-seq) on fLX from naïve BLT-L mice and at 2 and 12 dpi. While most cells detected in fLX by scRNA-seq were human, a minor population of mouse cells were detected, which were excluded from downstream analysis (**Fig. S3A-C**). Analysis of the human compartment revealed diverse immune subsets (T cells/innate lymphoid cells (ILC), B cells, myeloid cells and mast cells) and non-immune cell types (ciliated and non-ciliated epithelial, endothelial, mesenchymal cells and chondrocytes) in both

naïve and infected fLX (**Fig. 3A-C and Fig. S3D,E**). It is important to note that because our tissue digestion process and scRNAseq (in contrast to single nucleus RNAseq) both favor hematopoietic cell characterization compared to non-immune compartments (11, 12), the recovery of non-hematopoietic cell types is reduced, as evidenced by the limited number of cells in the epithelial compartment. Regardless, the transcriptomic dynamics within each cell type, including epithelium, could be examined upon infection.

Initial analysis showed that the transcriptomic response of the epithelial compartment upon infection was consistent with previously reported signatures of patients suffering from COVID-19 (*11-13*). Indeed, we noted a relative reduction of the alveolar type 2 (AT2) compartment at 2 dpi (25.6%) compared to naïve mice (73.1%), which was partially restored at 12 dpi (49.1%) (**Fig. 3D,E**). In contrast, the AT1 compartment increased at 2 dpi (9.89% compared to 8.00% in naïve fLX), consistently with the ability of AT2 cells to differentiate into AT1 upon lung damage (*14*). AT2 cells did not exhibit any robust antiviral responses (**Fig. 3F**) in accordance with the absence of viral RNA in this compartment (**Fig. 3G**). Given the clear evidence of epithelial infection in fLX at 2 dpi (**Fig. 1B^{b}**), the significant cytopathic damages induced by SARS-CoV-2 in AT2 cells (*15*), which results in a marked reduction of the AT2 compartment upon infection ((*16*) and **Fig. 3E**), likely precluded the isolation of infected AT2 cells following fLX digestion and single-cell isolation. However, bystander, non-infected AT2 cells displayed previously reported COVID-19 signatures found in humans, including downregulation of MHC genes (*HLA-C, HLA-B, and HLA-DPB1)* and *CCL5* (a cytokine associated with immune recruitment during respiratory infection) (**Fig. 3F**) (*17*). To summarize, fLX epithelium recapitulated previously reported features of COVID-19 in humans, including downregulation of immune genes and antigen presentation, and activation of tissue repair mechanisms.

Following epithelial benchmarking, we examined how the overall human immune system mobilizes within infected fLX. T-cells and innate lymphoid cells (ILC) have the same transcriptional programs, express TCR genes, and play similar effector functions (*18*). Their shared features

render them very challenging to distinguish by scRNAseq in small datasets and without TCR sequencing information (*19*). We thus considered them together as part of a T-cell/ILC population. T-cell/ILC frequency dramatically decreased in fLX upon infection (naïve, 66.8%; 2 dpi, 35.3%; 12 dpi, 21.8%), which is consistent with evidence that COVID-19 can induce lymphocyte depletion (**Fig. 3B,C**). Notably, lymphopenia was not observed in the peripheral blood of BLT-L mice, suggesting that lymphocyte depletion in fLX was not directly attributed to declining circulating peripheral lymphocytes (**Fig. S3F)**. In contrast, myeloid (naïve, 9.94%; 2 dpi, 25.3%; 12 dpi, 22.2%) and B-cell subsets (naïve, 3.64%; 2 dpi, 5.38%; 12 dpi, 5.31%) relatively expanded upon infection (**Fig. 3A-C**).

One myeloid and one T-cells/ILCs populations showed clear segregation by time point (population A and B in **Fig. 3B**) and were specific to 2 dpi. Most notably, these two hematopoietic sub-clusters were also highly enriched in viral RNA compared to other hematopoietic lineages (population A and B; **Fig. 3G, H**). While mesenchymal subsets also exhibited high levels of viral reads (**Fig. 3G**), reads were limited and distributed sporadically without significant enrichment within a given sub-cluster (**Fig. 3H and Fig. S3G**), including a 2 dpi-specific mesenchymal sub-cluster (Population C; **Fig. 2B**), underscoring a lack of association between viral RNA and mesenchymal activation upon SARS-CoV-2 challenge. Given their high enrichment in viral RNA and temporal association with acute viral replication, this initial transcriptomic analysis highlights the 2 dpi-specific myeloid and T-cells/ILCs populations identified as significant candidates in our search for the cellular mediators of infection resolution.

Inflammatory monocytes are major drivers of myeloid antiviral responses upon infection.

Next, we wished to examine more closely the transcriptomic profile of the viral RNA positive-myeloid and T/ILC populations. Since CD4+ cell depletion had a statistically significant impact on infection resolution compared to CD3+ cell depletion (**Fig. 2B**), and given that human monocytes, as well as some macrophages and dendritic cells (DC), also express CD4 (*20, 21*),

we first focused our study on the myeloid compartment. Sub-clustering of myeloid lineages unveiled diverse subpopulations, including alveolar and interstitial macrophages, various monocytes subsets, and one conventional DC subset (cDC) (**Fig. 4A and Fig. S4A-C**). Notably, we found the 2 dpi-specific viral RNA-enriched myeloid subset, earlier referred to as population B (**Fig. 4A-C and Fig. 3B,H**), to bear a signature of inflammatory monocytes (iMO) (**Fig. 4A,D-G and Fig. S4D**). iMO exhibited elevated expression of *VCAN, S100A8, CD14, CD163* and absence/minimal expression of *CD4, MARCO and CD206 (MRC1)* (**Fig. 4D-F and Fig. S4D)**.

Only iMO and alveolar macrophages increased in frequencies upon acute infection, whereas cDC and interstitial macrophage frequencies decreased (**Fig. 4G**). iMO were the most abundant lineage at 2 dpi (33.5%; **Fig. 4G**) and were the leading mediators of antiviral responses, as exemplified by the robust upregulated expression of interferon-stimulated genes (ISGs) and inflammatory cytokines (*CCL8, CXCL10, CCL2, ISG15, DEFB1, IL1RN, IFIT1, ISG20, IFIT3,* and *MX1*), as well as inflammatory markers such as *CD163* (**Fig. 4D,H**). While some ISGs (e.g., *ISG15, IFIT3, and MX1*) were expressed in other myeloid lineages at 2 dpi, their expression was markedly lower compared to iMO, suggesting a strong association between viral RNA and potentiated antiviral responses. Notably, upregulation of *CCL8*, *CXCL11* and *DEFB1* transcripts were the most exclusive to iMO (**Fig. 4H**).

As a side note, we also examined whether viral RNA-associated iMOs (CoV-iMOs) displayed a specific transcriptomic signature compared to iMOs (noCoV-iMOs) with undetectable viral RNA. Notably, only two genes correlated with the presence of viral RNA in iMOs: *FGL2 and C15orf48* (**Fig. 4I**). While *FGL2* was down-regulated in CoV-iMO compared to noCoV-iMOs, *C15orf48* was upregulated. Soluble FGL2 exerts immunosuppressive functions (notably by inhibiting the NF-kB pathway) (*22*). Conversely, the mitochondrial protein C15orf48 is positively regulated by NF-kB signaling (*23*) and has previously been implicated in severe COVID-19, acting as a positive regulator of inflammation (*24*).

These findings underscore CD163+ iMO as major mediators of antiviral responses within myeloid subsets and suggest that productive or abortive SARS-CoV-2 infection could further potentiate iMO inflammation through a specific set of genes.

iMO are extravascular and derive from patrolling CD4+ monocytes

As iMO could contribute to infection resolution in BLT-L mice, we sought to understand the origin of this transient cell subset using scRNA-seq, and cross-validate our findings using mIHC approaches. We found that low expression of *CD4* was a defining feature of iMO amongst monocyte sub-lineages (**Fig. 4E**), suggesting that iMO differentiation may be associated with loss of *CD4* expression. In parallel to this observation, we noted a large population of *CD4+ CD163-CD206(MRC1)*-patrolling intravascular monocyte (PIM) at all time points (**Sub-cluster 0**; **Fig. 4A,D-F**), with 2 dpi-specific PIM harboring a transcriptomic signature bridging naïve PIM and 2 dpi-specific iMO. At 12 dpi, PIM was the dominant subset over other monocyte subsets (50.3%; **Fig. 4G**). These results suggest that the infiltration and activation of PIM in fLX upon infection gives rise to a transient CD163+ iMO population contributing to infection resolution (**Fig. 4J**).

Analysis of myeloid chemotaxis transcriptomic signatures was consistent with increased monocyte infiltration into fLX upon infection. Productive infection of fLX at 2 dpi resulted in the emergence of cell subsets expressing high levels of human *CCL2* (**Fig. S4E**), which include our CD163+ iMO subset and a 2 dpi-specific T-cells/ILCs sub-cluster (population A in **Fig. 3B**). Activation of alveolar macrophages upon acute infection was also associated with increased *CCL2* expression by these cells (**Fig. S4E**). Several transcripts involved in myeloid chemotaxis, such as CXCR4 and MCAM (25, 26), were also upregulated in activated, 2 dpi-specific endothelial cell sub-cluster (**Fig. S4G-I**), underscoring the potential contribution of the endothelium in myeloid recruitment.

In support of our transcriptomic findings, mIHC analysis revealed that while naïve fLX displayed high numbers of CD3+ cells and detectable CD163+ interstitial cells (likely

macrophages), acute infection at 2 dpi showed an increase in CD4- CD163+ cells both in the extravascular interstitium and alveolar spaces (**Fig. 4K**). These dynamics mirrored the 2 dpi-specific expansion of CD4- CD163+ iMO and alveolar macrophages uncovered through scRNA-seq (**Fig. 4G**). A significant number of CD4+ CD3- CD163- cells were also apparent at that time point by mIHC (**Fig. 4K**), which is consistent with the identification of CD4+ CD163- PIM at 2 dpi by scRNAseq (**Fig. 4B,D,E**). Reduction of CD3+ T-cell was also apparent at 2 dpi (**Fig. 4K**) in accordance with our scRNAseq findings (**Fig. 3C**). At 12 dpi, CD3- CD4+ cells were still noted in fLX (**Fig. 4K**), reflecting the expansion of CD4+ PIM observed by scRNAseq (**Fig. 4G**). A significant number of CD163+ cells were still observed in fLX at that time point (**Fig. 4K**) but mainly concentrated in the interstitium, consistent with our scRNA findings that an increase in CD163+ interstitial macrophages may concur simultaneously with the reduction in CD163+ iMO numbers (**Fig. 4G**).

Concomitant to a recent study reporting that PIM give rise to a non-classical, extravascular monocyte population in the mouse lung that expand upon stimuli (*25*), our mIHC and scRNA-seq findings collectively suggest that infiltration of CD4+ PIM in infected fLX precede PIM extravasation and differentiation into extravascular iMO. In further support of this extravascular nature of iMO, the iMO gene expression profile was similar to those of human FCN1-monocytes recovered from the broncho-alveolar lavage of COVID-19 patients with acute respiratory disease syndrome (*26*), overall strengthening the non-classical, extravascular monocyte nature of iMO and their human relevance in COVID-19. Extravascular iMO are referred to as ExiMO in the rest of our study.

CD4+ cell depletion disrupts CD163+ cell recruitment into productively infected fLX.

Productive fLX infection at 2 dpi is associated with a significant increase in CD163+ cells in fLX (**Fig. 4K**), which is dominantly attributed to ExiMO differentiation as per our scRNA-seq data (**Fig. 4B,D**). At 12 dpi, the overall amount of CD163+ cells in fLX remained high (**Fig. 4K**)

and was not statistically different from the amount of CD163+ cells observed at 2 dpi (**Fig. 5A,B**), which is likely the manifestation of the presence of residual ExiMO and of the differentiation of CD163+ CD206+ interstitial macrophages from infiltrating CD4+ CD14+ CD16- monocytes at 12 dpi (**Fig. 4D,G**) consistently with the literature (*27*). As our data support a model in which infiltrating CD4+ PIM differentiate into CD163+ ExiMO and interstitial macrophages upon and following infection respectively, we examined how CD4+ cell depletion impacts CD163+ recruitment in fLX. Of note, because of the limited accessibility of fetal tissues and of a conscious choice to limit our use of such tissue as much as possible, we restricted our analysis to a single time point. We chose to focus our analysis on phenotypes observed at 12 dpi to ensure their association with persisting infection (in contrast to acute infection).

Following CD4+ cell depletion, persistently infected fLX displayed a significantly reduced number of CD163+ cells in fLX compared to isotype-treated and non-treated mice at 12 dpi (**Fig. 5A,B**). Expectedly, a major reduction was observed in the interstitial space (**Fig. 5A**), consistently with reduced numbers of ExiMO and interstitial macrophages. Limited numbers of alveolar CD163+ cells were still observed in the fLX of CD4+ cell-depleted mice co-localized with PPARγ (**Fig. 5A**), a marker of lung alveolar macrophages, which are unlikely to be depleted by anti-CD4 antibodies consistently with the known limited accessibility of alveolar macrophages to systemic antibodies (*28*). Despite being both similarly infected, fLX of acutely infected mice (2 dpi) also displayed significantly higher numbers of CD163+ cells than persistently infected fLX (12 dpi) (**Fig. 5A,B**). These findings support evidence that CD4+ cell depletion prevents monocyte infiltration into fLX during and following infection, and consequentially any differentiation into CD163+ cells. Notably, systemic levels of human CCL2 and CCL3, major monocyte attractants, were elevated in CD4+ cell-depleted mice and comparable to those of acutely infected mice (**Fig. 5C**), underlining how defective CD163+ recruitment stems from a lack of circulating CD4+ cells rather than reduced chemotaxis. Together, our findings therefore suggest that CD4+ cell depletion abrogates the recruitment of ExiMO in infected fLX.

Depletion of CD4+ cells in BLT-L mice promotes an immune tolerance state defined by the lack of CXCL10 production

To further support a link between CD4+ cell depletion, persistent infection and lack of ExiMO differentiation, we compared antiviral responses during acute and persistent infection. Among 32 cytokines and chemokines analyzed in the peripheral blood, CXCL10 was the only cytokine displaying significantly increased serum levels in acutely infected mice (2 dpi) prior to returning to undetectable levels upon infection resolution (12 dpi) (**Fig 5D**). However, interestingly, levels of circulating human CXCL10 in persistently infected CD4+ cell-depleted mice were not statistically different than those of mice that resolved infection (12 dpi) (**Fig 5D**), suggesting that CD4+ cell depletion promotes a state of immune tolerance that favors viral persistence. These findings also underscore systemic CXCL10 as a biomarker of viral clearance.

Several human subsets within fLX express *CXCL10* upon acute infection, including myeloid, mesenchymal and endothelial subsets (**Fig. S5A,B**). Among mesenchymal subsets, activated fibroblasts were enriched in *CXCL10* transcripts (**Fig. S5C-E**) unlike activated endothelial cells (**Fig. S4I**). However, the myeloid compartment was the major source of *CXCL10* among all human clusters at 2 dpi (**Fig. S5A,B**) and this phenotype was dominantly driven by ExiMO (**Fig. 4H, S5B**). These observations underscore ExiMO as the dominant producer of CXCL10 upon acute infection and as a significant source of this potential biomarker of infection resolution.

Taken together, our results suggest that CD4+ cell depletion prevents the induction of antiviral cytokines (i.e., CXCL10) dominantly expressed by ExiMO, resulting in a state of immune tolerance that likely favor viral persistence. Combined with evidence that such a depletion abrogates the recruitment of CD163+ cells into fLX upon infection and that ExiMO are the dominant CD163-expressing cell population differentiating upon acute infection, these findings collectively underscore ExiMO as critical mediators of infection resolution.

Persistent infection is associated with systemic and local signatures of chronic infection.

To probe whether CD4+ cell depletion and the lack of CD163+ cell recruitment drive long-lasting viral persistence instead of simply delaying infection resolution, we investigated whether immune tolerance in CD4+ cell-depleted mice is associated with signatures of chronic infection. Notably, persistently-infected mice antiviral responses were distinguishable from acutely infected (2 dpi) and isotype-treated (12 dpi) mice by elevated levels of CCL19 in serum (**Fig. 5E**). CCL19 is a pro-inflammatory cytokine that has been linked with persistent viral replication and inflammation such as in the context of HIV-1 infection (*29*), underlining that persistent SARS-CoV-2 infection in BLT-L mice recapitulate key immunological features of chronic viral infection.

We have previously reported that fLX exhibit significant histopathological manifestations of disease upon SARS-CoV-2 infection in the absence of an engrafted human immune system (3), highlighting that tissue damage in fLX is virally induced. However, persistent infection did not result in any significant histopathological manifestations of disease in fLX, which strongly contrasts with acutely infected fLX (**Fig. 1D, Fig. 5F**). As minimal tissue damage is a hallmark of chronic viral infection (*30*), these findings further support evidence that CD4+ cell depletion promotes tissue remodeling processes underlying chronic infection and lasting viral persistence.

Macrophage-like T-cells are enriched in viral RNA and mount robust antiviral signatures.

Lastly, we aimed to complete our study by characterizing the 2 dpi-specific T-cell/ILC sub-cluster emerging upon acute infection (population A in **Fig. 3B**), as CD3+ cell depletion had a moderate, albeit non-significant, impact on infection resolution (**Fig. 2B**). T-cell/ILC responses were limited to this specific subpopulation (**Fig. 6A,B**), which clustered very distinctively from other CD3+ T-cell lineages, including canonical CD4+ and CD8+ T-cells, and was highly enriched in viral RNA (Sub-cluster 6; **Fig. 6A-C**). Cells included in this subpopulation displayed low levels of CD4 and CD8 transcripts and elevated levels of mitochondrial transcripts **(Fig. 6E; Fig. S6A,B**).

Most notably, this T-cell/ILC subset was uniquely defined by the expression of several transcripts known to be enriched in macrophages (*MARCO*, *TIMP1*, *LYZ*), fibroblasts (*MGP*, *CALD1*, *COL1A*), or both (*A2M*, *IFITM3*) but not in T-cells (**Fig. 6E and Fig. S6D**). Cells included in this subset also exhibited evidence of cytotoxic function through the expression of *GZMA*, *GZMB*, and GNLY transcripts, albeit expression was also detected in CD8+ T-cells and activated tissue-resident memory T-cells (TRM) (Sub-clusters 1,3,4, **Fig. 3E and Fig. S3D**). Given the proximity of this sub-cluster with myeloid lineages (**Fig. 3A,B**) and evidence of expression of macrophage-enriched transcripts, we referred to this unique sub-cluster as Macrophage-like T-cells (MTC). MTC also exhibited upregulation of key gene pathways related to COVID-19, SARS-CoV-2 cell-intrinsic immune responses, cellular cytotoxicity (e.g., degranulation) and cell death, consistently with a role for this subset to serve as a robust primary responder to viral infection. (**Fig. 6D**). Collectively, these findings suggest a potential link between our CD3+ cell-depletion findings and the innate antiviral responses of CD3+ MTC.

DISCUSSION

As our appreciation of the immunological differences between mice and humans continues to grow, humanized mouse models are increasingly standing out as robust platforms to understand how viral pathogens interact with human tissues and the human immune system. These models are especially valuable when investigating tissue and mucosal immunity since such investigations remain impractical in human patients.

The SARS-CoV-2 pandemic has emphasized the need to increase our understanding of immune mechanisms that can drive protection against immunologically novel respiratory viruses. Mice engrafted with human immune systems and human lung tissues have emerged as valuable tools for such investigations (*2-5*), bridging the limitations of conventional animal models and the challenges associated with human studies. We previously reported using the HNFL mouse model that such models can be leveraged to capture immunological signatures defining effective control

of SARS-CoV-2 infection (*3*). However, the enhanced myeloid reconstitution of the HNFL model rapidly inhibits viral replication in fLX, precluding our ability to study protective naive immunological mechanisms at play upon acute and potentially symptomatic infection. This study aimed to uncover novel facets of these mechanisms using an alternative humanized mouse model that exhibits robust susceptibility to acute hERV infection and a robust ability to resolve infection in a hematopoietic-dependent manner.

We found that BTL-L mice are able to effectively clear both infectious viral particles and viral RNA following an early peak of viral replication in fLX. Systemic depletion of CD4+, but not CD3+ or CD8+ robustly abrogates infection resolution, underlining the contribution of the human hematopoietic compartment in this process. This is consistent with evidence that immunodeficient mice only engrafted with fLX are unable to clear infection (*3, 31*). Leveraging scRNAseq approaches, we uncovered ExiMO as a transient and novel subset of extravascular monocytes. ExiMO are directly related to CD4+ PIM and are the dominant CD163-expressing myeloid subset to emerge in fLX upon acute viral replication. They are also highly enriched in viral RNA and display unique antiviral and myeloid transcriptomic signatures. Notably, CD4+ cell depletion abrogates CD163+ infiltration in fLX despite persisting viral replication and promotes a state of immune tolerance defined by the lack of an antiviral cytokine, CXCL10, defining effective infection resolution and dominantly expressed by ExiMO. Lastly, we uncovered that CD4+ cell depletion is also associated with signatures of chronic infection systemically and in fLX.

All of our findings unequivocally converge toward a critical role of ExiMO in driving infection resolution in fLX. These cells belong to the only subset displaying the four following features: 1) a dominant CD163-expressing population that emerge during acute infection, 2) a major source of *CXCL10* expression, 3) a high enrichment in viral RNA and 4) the induction of robust antiviral responses. Our study therefore unravels ExiMO recruitment into lung tissues as a critical immunological process driving effective infection resolution and prevention of chronic infection. Notably and to the best of our knowledge, our study represents the first evidence of a lung

493 monocyte extravascular subset with antiviral functions. Extravascular monocytes are known to
494 originate from circulating patrolling monocytes and have been proposed to serve as immune
495 sentinels through their position at the interface of the lung capillaries and alveoli(*25, 32*). However,
496 although previous research reported that these cells can promote T-cell resident memory
497 differentiation following viral infection (*33*), their direct antiviral functions have not been
498 documented until now.
499
500 Our study collectively illuminates a novel immunological model that may–in part–define
501 naïve antiviral immunity against SARS-CoV-2 and potentially other hERVs in the human lung
502 (**See Graphical Abstract**). We propose that upon infection of fLX, initial epithelial infection
503 triggers the activation of fibroblasts and endothelial cells. While fibroblasts potentiate initial
504 myeloid inflammatory responses, endothelial activation, and CCL2 production by several
505 activated subsets (of mesenchymal and myeloid origin) promote PIM infiltration into fLX. Following
506 extravasation, PIM then subsequently differentiate into ExiMO, which may exert a bimodal
507 function: they drive tissue-wide antiviral responses protecting the epithelial compartment from
508 persistent infection, and phagocyte viral particles and components, heightening their antiviral
509 responses. Infection resolution is associated with a significant reduction of ExiMO in fLX,
510 subsequent infiltration of PIM and differentiation into CD206+ interstitial macrophages which
511 promote tissue repair. By preventing PIM infiltration into fLX and subsequent ExiMO differentiation
512 and antiviral responses, CD4+ cell depletion promotes a state of immune tolerance driving long-
513 lasting viral persistence.
514 Through such model, our findings significantly enhance a recent human study reporting
515 that protection from SARS-CoV-2 infection is associated with a rapid monocyte response in the
516 nasal cavity and a decreased number of circulating monocytes(*1*). Specifically, our work extends
517 the findings of this human study beyond the limitations of the human model by exploring tissue-
518 resident events, unraveling the identity of monocyte populations that extravasate tissues,

519 differentiate and mount tissue-resident immune responses to clear infection. By providing
520 enhanced resolution on key protective immunological processes and mediators that human
521 studies alone cannot capture, underscoring how human and humanized mouse studies can
522 effectively complement themselves for improving our understanding of human antiviral immunity.
523
524 While our study emphasizes the protective role of monocytes in preventing severe COVID-
525 19, monocytic lineages have also been extensively associated with severe COVID-19 (*11-13, 26*).
526 Excessive monocyte infiltration, macrophage inflammation and fibrotic response can lead to
527 potentially fatal acute respiratory distress syndrome (ARDS) and fibrosis despite promoting
528 infection resolution. A suspected driver of excessive myeloid inflammation is the ability of SARS-
529 CoV-2 to trigger abortive infection of both monocytes and macrophages (*34-37*) through viral RNA
530 replication and protein production, which results in inflammasome activation (*37-39*). However,
531 viral RNA in ExiMO is associated with rapid infection resolution and tissue protection. These
532 findings suggest that monocytic infection can also be associated with positive clinical outcomes
533 and that the inflammatory trajectory of infected monocytes may define the course of COVID-19.
534 By 12 dpi and infection resolution, fLX displayed residual ExiMO and were enriched in
535 CD4+ PIM and CD163+ CD206+ interstitial macrophages. These findings are consistent with
536 mouse studies reporting that CD206+ interstitial macrophages are involved in response to
537 wounding and infection recovery, while CD206- interstitial macrophages are primary responders
538 to infection and more pro-inflammatory (*25*). However, human patients experiencing severe
539 COVID-19 and ARDS display an accumulation of pro-fibrotic CD163+ CD206+ monocyte-derived
540 interstitial macrophages (*26*). These cells have been shown to directly derive from extravasating,
541 circulating CD14+ monocytes in another human immune system-engrafted mouse model(*27*),
542 suggesting that exacerbated monocyte infiltration and differentiation into CD206+ interstitial
543 macrophages are a significant driver of COVID-19 disease as viral infection is being cleared in
544 lung tissues. In addition to this, other studies have reported that PIM can give rise to lung

545 extravascular monocytes in mice (*25*). These cells exhibit a dynamic transition state and can
546 differentiate into CD206- interstitial macrophages. However, notably, no CD206- macrophages
547 were observed in infected fLX at any time point. Together, these findings suggest that the absence
548 of ExiMO differentiation into CD206- interstitial macrophages during infection represents a
549 defining hallmark of protection from severe COVID-19. Limited differentiation would avert
550 uncontrolled and imbalanced inflammation during infection resolution, preventing severe tissue
551 damage and subsequent exacerbated monocyte differentiation into pro-fibrotic CD206+ interstitial
552 macrophages (**Figure 7**). Together, our study suggests that ExiMO antiviral responses represent
553 a critical crossroad that can shape the clinical trajectory of SARS-CoV-2 infection.
554
555 Our findings call for numerous follow-up investigations. Understanding the cellular and
556 molecular actors defining the fate of ExiMO upon exposure to SARS-CoV-2 and how key
557 regulatory crossroads in this subset may result in differential clinical outcomes is of particular
558 interest. Compounding immune dysregulations, such as elevated inflammatory baseline and/or
559 specific myeloid imprinting, may contribute to PIM and/or ExiMO's inability to adequately regulate
560 their activation in a timely manner upon encountering viral materials or inflammatory clues,
561 leading to rapid differentiation into macrophages and exacerbated inflammation. Our study also
562 creates a mandate for probing the ubiquitous nature of ExiMO antiviral responses during other
563 respiratory viral infections and investigating more comprehensively the antiviral functions of this
564 novel subset beyond SARS-CoV-2 infection. Investigating the contribution of endothelial
565 activation in driving effective monocyte infiltration and infection resolution, as well as these cells'
566 contribution to ExiMO differentiation, is also of particular significance. It remains unclear as to
567 how endothelial and fibroblasts are activated during infection as neither cell population displayed
568 signs of viral RNA enrichment. Whether activation of these cells is triggered indirectly by early
569 epithelial and/or myeloid activation, or via direct exposure to viral components such as the
570 nucleocapsid protein (*40*) could be investigated using the BLT-L mouse model.

In parallel to ExiMO, we also identified MTC, a transient T-cell population highly enriched in viral RNA and only observed upon acute infection. MTC exhibited expression of key macrophage-defining genes and elevated cytotoxic activity. While this population presents some similarity with innate-like T-cells (*41*), which harbor cytotoxic signatures and whose roles in cancer have been investigated, MTC appear to be unique given their combination of lymphoid, myeloid and mesenchymal markers and their short-lived, apoptotic nature suggested by their complete absence at 12 dpi. MTC also share transcriptomic similarities with γδ T-cell subsets previously described as bearing myeloid and cytotoxic functions (*42, 43*). However, their expression of conventional macrophage makers emphasizes their uniqueness. While CD8+ T-cells and macrophages isolated from nasopharyngeal swabs have been identified to harbor SARS-CoV-2 RNA in human challenge studies(*1*), MTC did not meet the canonical transcriptomic signatures of these subsets, suggesting the existence of tissue-resident events driving specific cellular differentiation processes upon infection. Additional investigations are required to better understand the identity, fate and functions of this novel cell subset in lung antiviral immunity. However, it is tempting to speculate that MTC may uniquely synergize CD8+ cytotoxic T-cell functions with viral particle phagocytosis to effectively control infection prior to undergoing rapid cell death.

Despite our findings related to MTC, the contribution of T-cells in SARS-CoV-2 infection resolution remains elusive in our model. CD3+ cell depletion resulted in a partial abrogation of infection resolution, with 50% of animals still capable of clearing infection. In addition, even when viral infection persisted in CD3+ cell-depleted animals, viral titers in fLX remained significantly lower than in the fLX of persistently infected CD4+ cell-depleted animals (**Fig. S2B**). One possible interpretation is that T-cell depletion delays but does not abolish infection resolution. CD8+ cell-depleted mice may display delayed viral clearance compared to isotype-treated mice (with resolution occurring between 6 dpi and 12 dpi), and CD3+ T-cell-depleted mice may be

undergoing progressive resolution by 12 dpi until complete clearance by a later time. In contrast, the viral titer observed in fLX of CD4+ cell-depleted mice show no evidence of ongoing infection resolution. How CD3+ depletion may impact MTC differentiation, and how T-cells (including MTC) and ExiMO functions may synergize to rapidly resolve infection without extensive inflammation-induced tissue damage will need further investigation.

There are inherent limitations associated with the BLT-L mouse model. First, direct viral inoculation into fLX potentially bypasses key immune checkpoints in the upper respiratory tract, which are not recapitulated in our model. Second, the hematopoietic reconstitution and functions of the BLT-L mouse model remain imperfect, notably through the underrepresentation of specific hematopoietic subsets, including dendritic cells and granulocytes, and limited B-cell responses – which may ultimately bias the dynamics of viral clearance. Despite these limitations, BLT-L mice recapitulated human lung responses to SARS-CoV-2 infection through AT2 loss of programming, fibroblast and endothelial activation, effective clearance of infection through robust hematopoietic responses. This mouse model also supported viral adaptation processes with public health relevance, and recapitulated signatures of persistent viral replication observed in patients suffering from chronic infection. Our work demonstrates the potential of the BLT-L mouse model to uncover naïve immune mechanisms and mediators governing the effective resolution of lung infection by SARS-CoV-2. Our findings open avenues for a comprehensive examination of the antiviral roles of ExiMO against hERV, which may pave the way toward innovative immunotherapy strategies against these pathogens.

AUTHOR CONTRIBUTIONS

D.K., A.B.B. and F.D. conceptualized the overall study. C.H. conceptualized the computational component of this study and oversaw the analysis of the single-cell RNA sequencing data. D.K., A.B.B., N.A.C. and F.D. designed the experiments. D.K., A.K.O., M.S, A.N, H.P.G., M.E., V.V.,

A.B.B. and F.D. performed experiments. D.K., A.K.O., A.T., J.T., M.S, A.N, P.M., M.E., J.H.C., V.V., N.A.C., C.H., A.B.B. and F.D. analyzed the data. J.T and C.H. carried out computational analysis. M.E. carried out electron microscopy analysis. A.B.B. and V.V. provided access to key resources. D.K. and F.D. wrote the manuscript with contributions from all authors.

ACKNOWLEDGMENTS

This work was supported in part by a start-up fund and Peter Paul Career Development Professorship from Boston University (to F.D.), grants from the National Institutes of Health (K22 AI144050 to F.D.), Clinical and Translational Science Awards (grant UL1 TR001430) from the National Center for Advancing Translational Sciences of the National Institutes of Health (to F.D., N.A.C. and A.E.), and an Evergrande MassCPR award (to R.B.). A.B.B. was supported by R01AI174875, R01AI174276, DP2DA040254, as well as CDC subcontract 200-2016-91773-T.O.2. and a Massachusetts Consortium on Pathogenesis Readiness (MassCPR) grant. We also thank the Evans Center for Interdisciplinary Biomedical Research at Boston University Chobanian and Avedisian School of Medicine for their support of the Affinity Research Collaborative on 'Respiratory Viruses: A Focus on COVID19'. This work utilized a Ventana Discovery Ultra and Akoya PhenoImager HT that were purchased with funding from National Institutes of Health SIG grants (S10 OD026983 & S10OD030269). We thank Ronald B. Corley, NEIDL director at the time of this study and MassCPR award recipient, for his constant encouragement and support for this study. We thank the Boston University Animal Science Center, the Ragon Institute Human Immune System Mouse core, the single cell sequencing core and microarray and sequencing core, and the flow cytometry core at Boston University Chobanian and Avedisian School of Medicine, and all the NEIDL animal core staff for their outstanding support. We also thank all the Douam, Balazs, Connor and Crossland lab members, NEIDL members, and members of the department of Virology, Immunology, and Microbiology and Pathology at Boston University for

their constant support and advice. D.K. is supported by a T32 training grant in immunology (T32AI007309).

MATERIALS AND METHODS

Detailed descriptions of the materials and methods used for this study are in the Supplemental Materials.

Study design. Three independent cohorts of BLT-L mice co-engrafted with human fLX, liver, thymus and hematopoietic stem cells from three distinct donors were generated for this study. Animals were challenged with SARS-CoV-2 (10^6 PFU) through direct fLX inoculation, and euthanized on day 2, 6 or 12 post-infection for blood and fLX collection. Naïve mice were used as negative controls. fLX were then processed for viral titer quantification, H&E staining and mIHC, scRNAseq and viral genome sequencing. Blood was processed for flow cytometry (for depletion experiments only) and serum cytokine analysis. For CD3+, CD4+ and CD8+ cell depletion, mice were treated with depleting antibodies prior and during infection through intraperitoneal injection.

Institutional approvals. All experiments in this study, including those conducted in BSL-3, were approved by an institutional biosafety committee. Animal experiments described in this study were performed in accordance with protocols that were reviewed and approved by the Institutional Animal Care and Use and Committee of the Ragon Institution and Boston University. All mice were maintained in facilities accredited by the Association for the Assessment and Accreditation of Laboratory Animal Care (AAALAC). All replication-competent SARS-CoV-2 experiments were performed in a biosafety level 3 laboratory (BSL-3) at the Boston University National Emerging Infectious Diseases Laboratories (NEIDL).

673

674 ***Mouse strains and sex as biological variable.*** Female NOD.Cg.-*Prkdc*^{Scid}*Il2rg*^{tm1Wjl}/SzJ (NSG)
675 mice were obtained from the Jackson Laboratory, catalog number 005557. NSG mice were
676 maintained by the Ragon Institute Human Immune System Mouse core prior to engraftment and
677 shipment to the NEIDL, Boston University. In our study, only female mice were engrafted with
678 human fetal tissues because of their ability to support higher levels of engraftment than males.
679 As we investigated human tissue responses to infection and only leveraged mice as
680 xenorecipients, the sex of the animals does represent a critical variable for our study.

681

682 ***Human fetal tissues.*** De-identified human fetal tissues were procured from Advanced Bioscience
683 Resources (Alameda, CA, USA).

684

685 ***Generation of BLT-L mice.*** BLT mice were generated via irradiation of female NOD.Cg.-
686 *Prkdc*^{Scid}*Il2rg*^{tm1Wjl}/SzJ mice (NSG mice; Jackson Laboratory #005557) prior to implantation of
687 human fetal thymic and fetal liver tissue (Advanced Bioscience Resources) under the murine
688 kidney capsula. Two pieces of homologous human fetal lung tissue were implanted into
689 subcutaneous dorsal pockets of mice. Post-implantation, mice intravenously received 1x10^5
690 homologous CD34+ cells. Human immune reconstitution was determined by flow cytometry at
691 weeks post-implantation. Three distinct human donors were used for this study.

692

693 ***Mouse inoculation with SARS-CoV-2.*** BLT-L mice were anesthetized with 1–3% isoflurane prior
694 to inoculation via subcutaneous, intra-fetal lung xenograft (intra-fLX) injection with 10^6 plaque
695 forming unites (PFU) of SARS-CoV-2 WA-1 isolate in 50 µL of sterile 1X PBS. Mice were
696 euthanized at 2-, 6-, and 12-days post inoculation.

697

In vivo antibody depletion. BLT-L mice were administered 200 mg of anti-CD3e (OKT3) (BioxCell; cat. # BE0001-2), anti-CD4 (OKT4) (BioxCell; cat. # BE0003-2), anti-CD8 (OKT8) (BioxCell; cat. # BE0004-2), or isotype IgG2a (Thermofisher; cat # 02-6200) antibody 3-, 2-, and 1-day prior to inoculation and 4- and 8-days post inoculation with $1x10^6$ PFU SARS-CoV-2 WA-1.

Quantification and statistical Analysis. For histopathological score and viral load/titer comparisons a Kruskla-Wallis, non-parametric one-way ANOVA with Benjamini, Krieger, and Yekutieli correction for multiple comparisons was applied given the non-continuous nature of the data. For cytokine data, an Ordinary one-way ANOVA with uncorrected Fishers LSD was used as the data was collected from different time points, treatment conditions, and cohorts. A Kruskla-Wallis, non-parametric one-way ANOVA with an uncorrected Dunn's test was applied for CD163+ Area quantification (AQ) due to the independent comparisons between the samples. All statistical tests and graphical depictions of results were performed using GraphPad Prism version 9.0.1 software (GraphPad Software, La Jolla, CA). For all tests, $p \leq 0.05$ was considered statistically significant. Statistical significance on figures and supplemental figures is labeled with p-values and non-significant values are labeled with n.s. or left unlabeled.

Data availability. The accession number for the raw data of the bulk and single-cell RNA-Seq is GSE255200.

REFERENCES

1. R. G. H. Lindeboom *et al.*, Human SARS-CoV-2 challenge uncovers local and systemic response dynamics. *Nature*, (2024).
2. Y. Di *et al.*, SARS-CoV-2 Variant-Specific Infectivity and Immune Profiles Are Detectable in a Humanized Lung Mouse Model. *Viruses* **14**, (2022).
3. D. J. Kenney *et al.*, Humanized mice reveal a macrophage-enriched gene signature defining human lung tissue protection during SARS-CoV-2 infection. *Cell Rep* **39**, 110714 (2022).

4. R. Sun *et al.*, Humanized mice for investigating SARS-CoV-2 lung infection and associated human immune responses. *Eur J Immunol* **52**, 1640-1647 (2022).
5. A. Wahl *et al.*, Precision mouse models with expanded tropism for human pathogens. *Nat Biotechnol* **37**, 1163-1173 (2019).
6. A. K. O'Connell, F. Douam, Humanized Mice for Live-Attenuated Vaccine Research: From Unmet Potential to New Promises. *Vaccines (Basel)* **8**, (2020).
7. PMDA, Xevudy for Intravenous Infusion 500 mg_GlaxoSmithKline K.K._Report on Special Approval for Emergency; https://www.pmda.go.jp/files/000245006.pdf. (2021).
8. A. Fagre *et al.*, SARS-CoV-2 infection, neuropathogenesis and transmission among deer mice: Implications for spillback to New World rodents. *PLoS Pathog* **17**, e1009585 (2021).
9. N. Arshad *et al.*, SARS-CoV-2 accessory proteins ORF7a and ORF3a use distinct mechanisms to down-regulate MHC-I surface expression. *Proc Natl Acad Sci U S A* **120**, e2208525120 (2023).
10. J. S. Yoo *et al.*, SARS-CoV-2 inhibits induction of the MHC class I pathway by targeting the STAT1-IRF1-NLRC5 axis. *Nat Commun* **12**, 6602 (2021).
11. T. M. Delorey *et al.*, COVID-19 tissue atlases reveal SARS-CoV-2 pathology and cellular targets. *Nature*, (2021).
12. A. F. Rendeiro *et al.*, The spatial landscape of lung pathology during COVID-19 progression. *Nature* **593**, 564-569 (2021).
13. E. Wauters *et al.*, Discriminating mild from critical COVID-19 by innate and adaptive immune single-cell profiling of bronchoalveolar lavages. *Cell Res* **31**, 272-290 (2021).
14. A. Wu, H. Song, Regulation of alveolar type 2 stem/progenitor cells in lung injury and regeneration. *Acta Biochim Biophys Sin (Shanghai)* **52**, 716-722 (2020).
15. J. Huang *et al.*, SARS-CoV-2 Infection of Pluripotent Stem Cell-Derived Human Lung Alveolar Type 2 Cells Elicits a Rapid Epithelial-Intrinsic Inflammatory Response. *Cell stem cell* **27**, 962-+ (2020).
16. J. C. Melms *et al.*, A molecular single-cell lung atlas of lethal COVID-19. *Nature* **595**, 114-119 (2021).
17. M. Liao *et al.*, Single-cell landscape of bronchoalveolar immune cells in patients with COVID-19. *Nat Med* **26**, 842-844 (2020).
18. C. Harly, M. Cam, J. Kaye, A. Bhandoola, Development and differentiation of early innate lymphoid progenitors. *J Exp Med* **215**, 249-262 (2018).
19. G. Pizzolato *et al.*, Single-cell RNA sequencing unveils the shared and the distinct cytotoxic hallmarks of human TCRVdelta1 and TCRVdelta2 gammadelta T lymphocytes. *Proc Natl Acad Sci U S A* **116**, 11906-11915 (2019).
20. A. Zhen *et al.*, CD4 ligation on human blood monocytes triggers macrophage differentiation and enhances HIV infection. *J Virol* **88**, 9934-9946 (2014).
21. L. Jardine *et al.*, Rapid detection of dendritic cell and monocyte disorders using CD4 as a lineage marker of the human peripheral blood antigen-presenting cell compartment. *Front Immunol* **4**, 495 (2013).
22. L. Fu, Z. Liu, Y. Liu, Fibrinogen-like protein 2 in inflammatory diseases: A future therapeutic target. *Int Immunopharmacol* **116**, 109799 (2023).
23. Y. Takakura *et al.*, Mitochondrial protein C15ORF48 is a stress-independent inducer of autophagy that regulates oxidative stress and autoimmunity. *Nat Commun* **15**, 953 (2024).
24. S. A. Clayton *et al.*, Inflammation causes remodeling of mitochondrial cytochrome c oxidase mediated by the bifunctional gene C15orf48. *Sci Adv* **7**, eabl5182 (2021).
25. J. Schyns *et al.*, Non-classical tissue monocytes and two functionally distinct populations of interstitial macrophages populate the mouse lung. *Nat Commun* **10**, 3964 (2019).
26. D. Wendisch *et al.*, SARS-CoV-2 infection triggers profibrotic macrophage responses and lung fibrosis. *Cell* **184**, 6243-6261 e6227 (2021).

27. E. Evren *et al.*, Distinct developmental pathways from blood monocytes generate human lung macrophage diversity. *Immunity* **54**, 259-275 e257 (2021).
28. T. Hussell, T. J. Bell, Alveolar macrophages: plasticity in a tissue-specific context. *Nat Rev Immunol* **14**, 81-93 (2014).
29. J. K. Damas *et al.*, Homeostatic chemokines CCL19 and CCL21 promote inflammation in human immunodeficiency virus-infected patients with ongoing viral replication. *Clin Exp Immunol* **157**, 400-407 (2009).
30. E. I. Zuniga, M. Macal, G. M. Lewis, J. A. Harker, Innate and Adaptive Immune Regulation During Chronic Viral Infections. *Annu Rev Virol* **2**, 573-597 (2015).
31. A. Wahl *et al.*, SARS-CoV-2 infection is effectively treated and prevented by EIDD-2801. *Nature* **591**, 451-457 (2021).
32. M. P. Rodero *et al.*, Immune surveillance of the lung by migrating tissue monocytes. *Elife* **4**, e07847 (2015).
33. P. R. Dunbar *et al.*, Pulmonary monocytes interact with effector T cells in the lung tissue to drive T(RM) differentiation following viral infection. *Mucosal Immunol* **13**, 161-171 (2020).
34. J. Zheng *et al.*, Severe Acute Respiratory Syndrome Coronavirus 2-Induced Immune Activation and Death of Monocyte-Derived Human Macrophages and Dendritic Cells. *J Infect Dis* **223**, 785-795 (2021).
35. A. Boumaza *et al.*, Monocytes and Macrophages, Targets of Severe Acute Respiratory Syndrome Coronavirus 2: The Clue for Coronavirus Disease 2019 Immunoparalysis. *J Infect Dis* **224**, 395-406 (2021).
36. D. Yang *et al.*, Attenuated Interferon and Proinflammatory Response in SARS-CoV-2-Infected Human Dendritic Cells Is Associated With Viral Antagonism of STAT1 Phosphorylation. *J Infect Dis* **222**, 734-745 (2020).
37. C. Junqueira *et al.*, FcgammaR-mediated SARS-CoV-2 infection of monocytes activates inflammation. *Nature* **606**, 576-584 (2022).
38. D. Munnur *et al.*, Altered ISGylation drives aberrant macrophage-dependent immune responses during SARS-CoV-2 infection. *Nat Immunol* **22**, 1416-1427 (2021).
39. E. Sefik *et al.*, Inflammasome activation in infected macrophages drives COVID-19 pathology. *Nature* **606**, 585-593 (2022).
40. Y. Qian *et al.*, Direct Activation of Endothelial Cells by SARS-CoV-2 Nucleocapsid Protein Is Blocked by Simvastatin. *J Virol* **95**, e0139621 (2021).
41. M. Molgora, M. Colonna, Innate-like T cells: A promising asset in anti-cancer immunity. *Cancer Cell* **40**, 714-716 (2022).
42. M. Lebedev, B. Faburay, J. A. Richt, A. Young, Myeloid-like gammadelta T cell subset in the immune response to an experimental Rift Valley fever vaccine in sheep. *Vet Immunol Immunopathol* **233**, 110184 (2021).
43. M. Muto, M. Baghdadi, R. Maekawa, H. Wada, K. Seino, Myeloid molecular characteristics of human gammadelta T cells support their acquisition of tumor antigen-presenting capacity. *Cancer Immunol Immunother* **64**, 941-949 (2015).

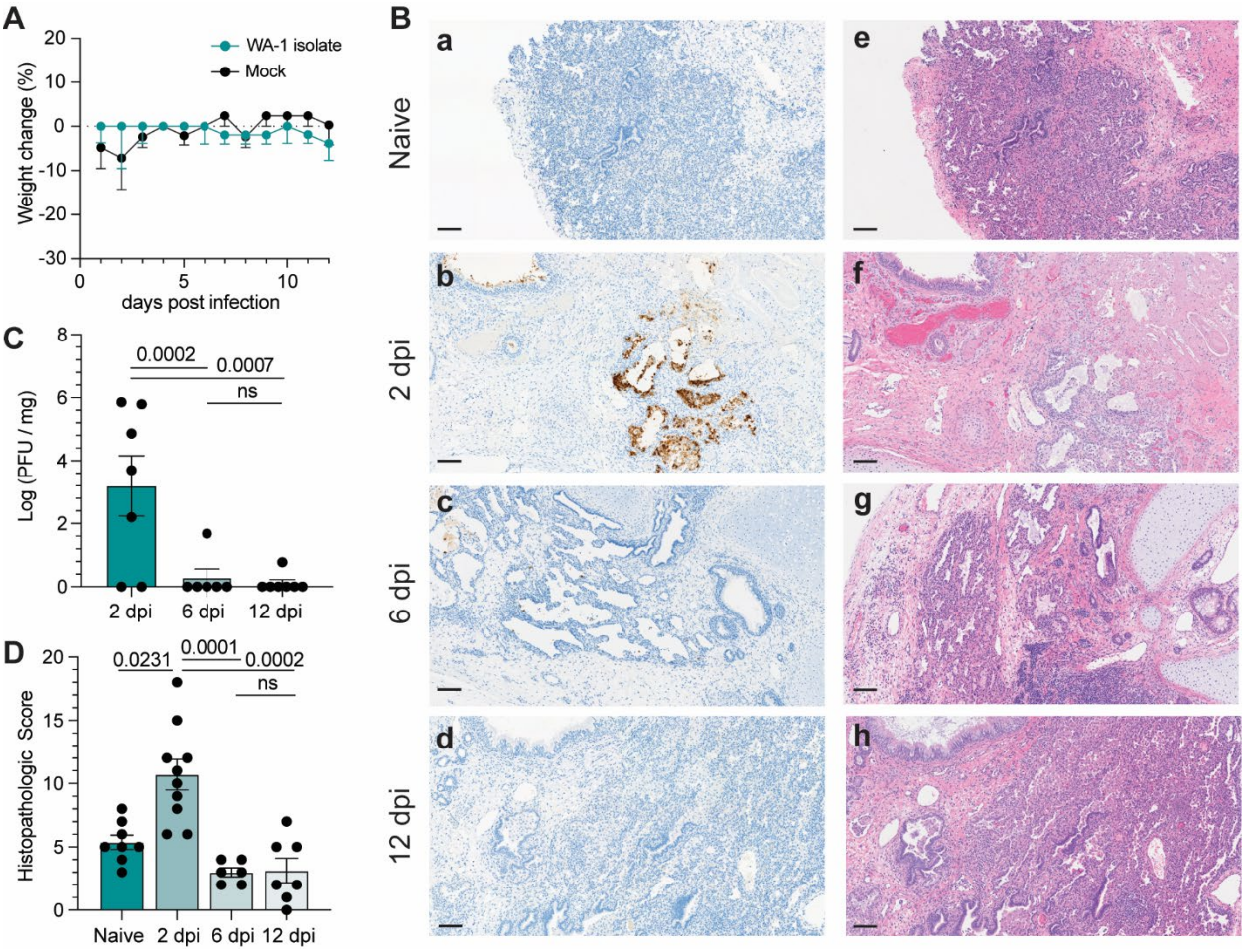

Figure 1. BLT-L mice effectively resolve SARS-CoV-2 infection and repair lung tissue. Fetal lung xenografts (fLX) of BLT-L mice were infected with 1x10^6 PFU of SARS-CoV-2 WA-1 isolate via subcutaneous intra-graft injection. **(A)** BLT-L mice were monitored for weight change over the course of 12-days post infection (dpi). **(B)** Immunohistochemistry for SARS-CoV-2 S protein **(a-d)** and hematoxylin and eosin staining **(e-f)** were performed on naïve fLX **(a,e)** and fLX at 2 dpi **(b,f)**, 6 dpi **(c,g),** and 12 dpi **(d,h)**. Scale bar = 100 μM **(C)** Viral titer (log(PFU/mg)) in fLX at 2, 6, and 12 dpi as determined by plaque assay. **(D)** Histopathological scoring of naïve fLX and fLX at 2, 6, and 12 dpi. Data are representative of two or three independent experiments. n = 6 -10 per timepoint. Error bars represent mean ± standard error of the mean. *One-way ANOVA analysis was performed. p-values are indicated. n.s. = non-significant.*

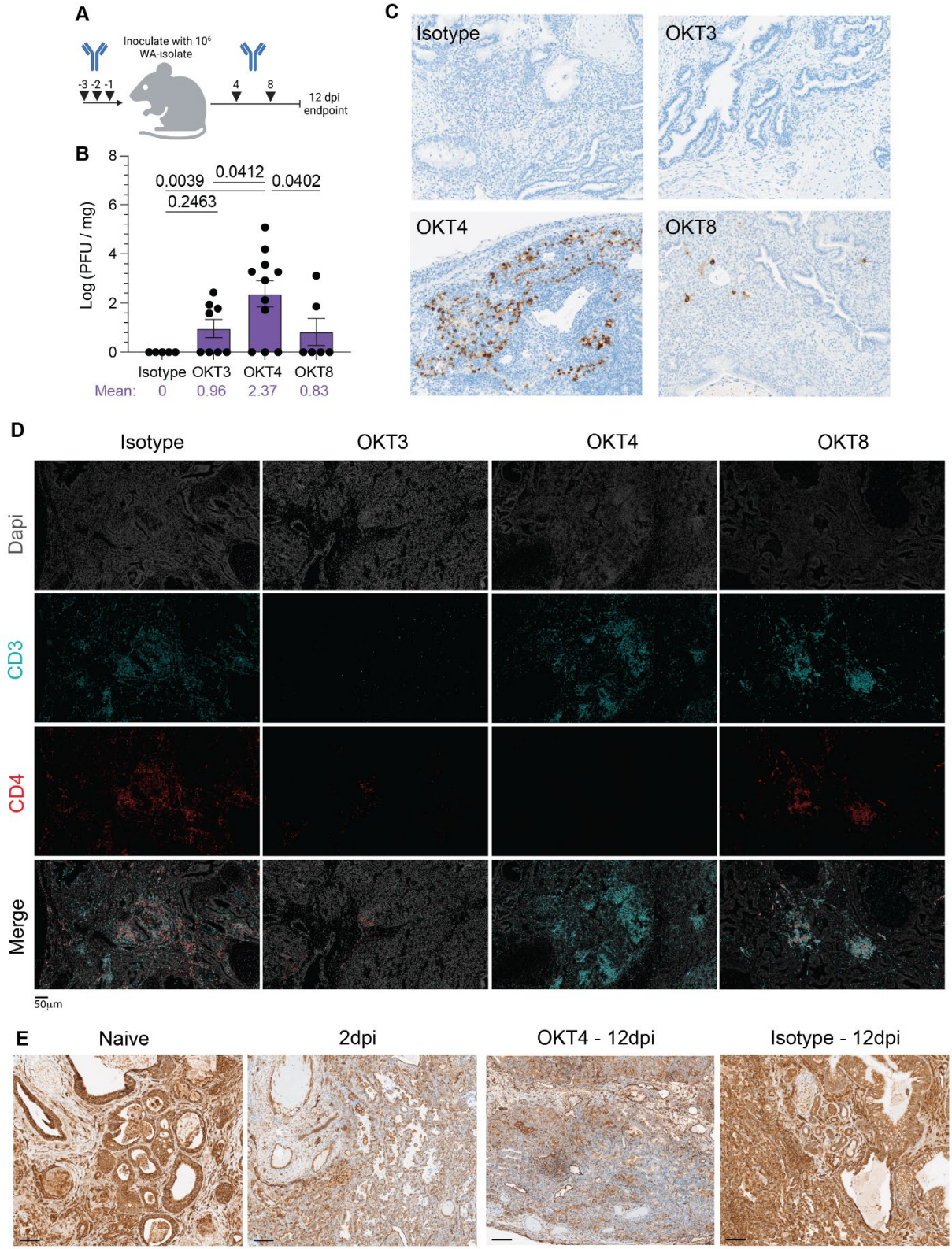

831

Figure 2. Systemic depletion of CD4+ cells results in persistent infection of fLX. (A) BLT-L mice were administered 200 μg of anti-CD3e (OKT3), anti-CD4 (OKT4), anti-CD8 (OKT8) or IgG2a isotype. **(B)** Viral titer (log(PFU/mg)) in fLX extracted from BLT-L mice treated with isotype, OKT3, OKT4, or OKT8 antibody at 12 dpi. **(C)** Immunohistochemistry for SARS-CoV-2 N protein on fLX of depleted or non-depleted BLT-L mice at 12 dpi. **(D)** Multiplex immunohistochemistry on fLX of depleted or non-depleted BLT-L mice at 12 dpi. Dapi = gray, CD3 = teal, CD4 = red. Scale bar = 50 μm. **(E)** MHC-I staining of fLX tissue sections (anti-MHC class I (EMR8-5) CST 88274) extracted from naïve mice, OKT4-treated mice (12 dpi), or from infected fLX at 2 and 12 dpi. Scale bar = 100 μM

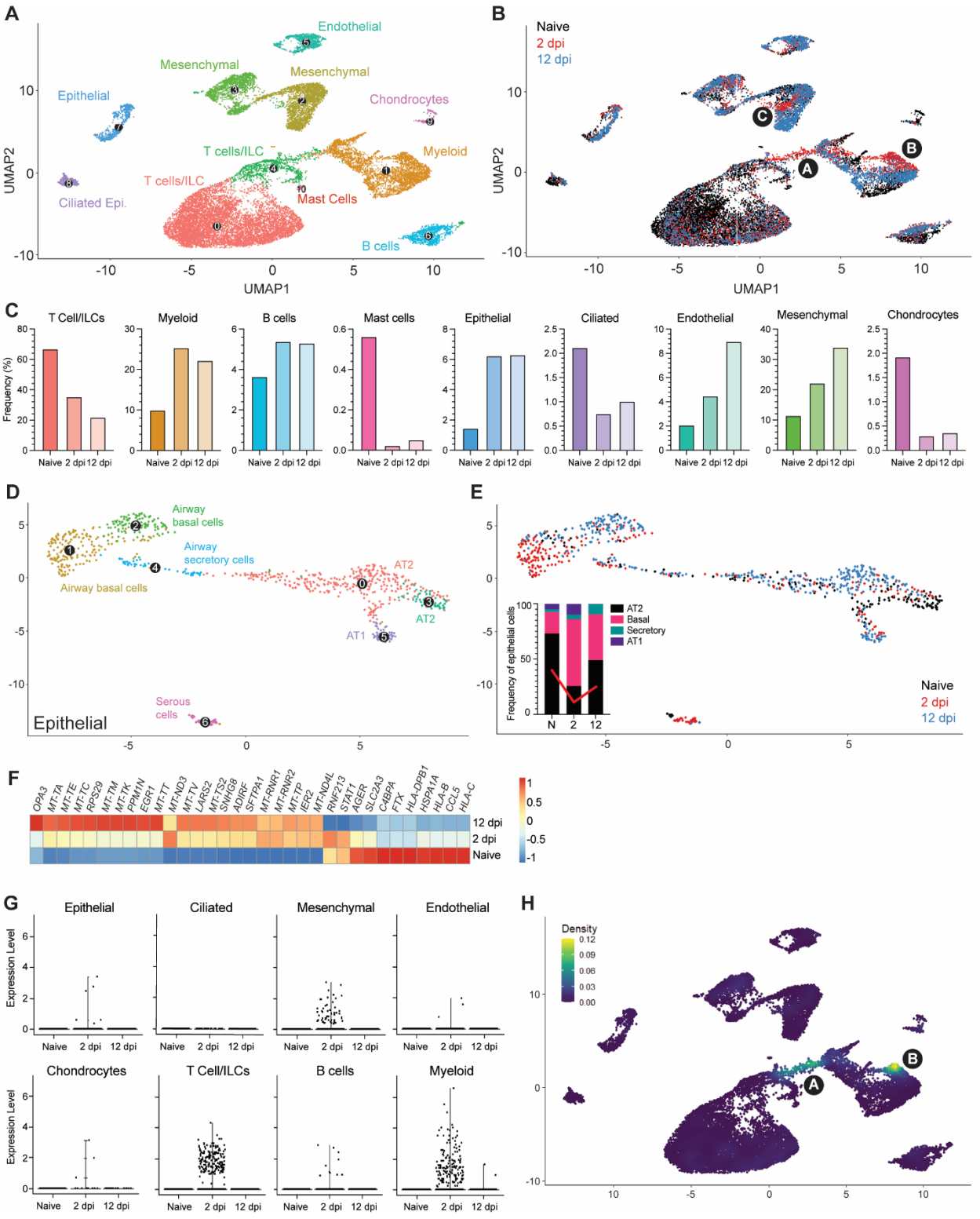

857

858

859

Figure 3. **Cellular remodeling and viral dynamics in fLX upon SARS-CoV-2 infection**

Single cell RNA sequencing analysis was performed on single cell suspensions of naïve fLX and fLX at 2 and 12 dpi. Naïve n=3 fLX (9,605 cells), 2 dpi n=2 fLX (4,405 cells), and 12 dpi n = 2 fLX (5,857 cells). **(A)** UMAP plot clustering of the human cell compartment of naïve fLX and fLX at 2 and 12 dpi. **(B)** Temporal annotation of the human clusters on the UMAP plot: naïve (black), 2 dpi (red), 12 dpi (blue). Sub-clusters unique to 2 dpi are annotated by A (T cell compartment), B (myeloid compartment) and C (mesenchymal compartment). **(C)** Frequency of each cell compartment determined by single cell RNA-sequencing. **(D)** Dot plots displaying the expression of SARS-CoV-2 viral RNA transcripts identified in scRNA-seq. **(E)** UMAP plot showing the distribution of SARS-CoV-2 viral RNA transcripts across all human cell clusters and time points. **(F)** UMAP plot sub-clustering of the human AT2 compartment in fLX across all time points. **(G)** Temporal annotation of the human epithelial sub-clusters on the UMAP plot: naïve (black), 2 dpi (red), 12 dpi (blue). The inset graph indicates the change in frequency of each compartment (AT2; black, Basal; pink, Secretory; teal, and AT1; purple) within the epithelial compartment. Red line indicates the change in the AT2 compartment over time. **(H)** Heatmap displaying the relative expression (from -1 to 1) of the top differentially regulated genes over the course of infection within the AT2 compartment.

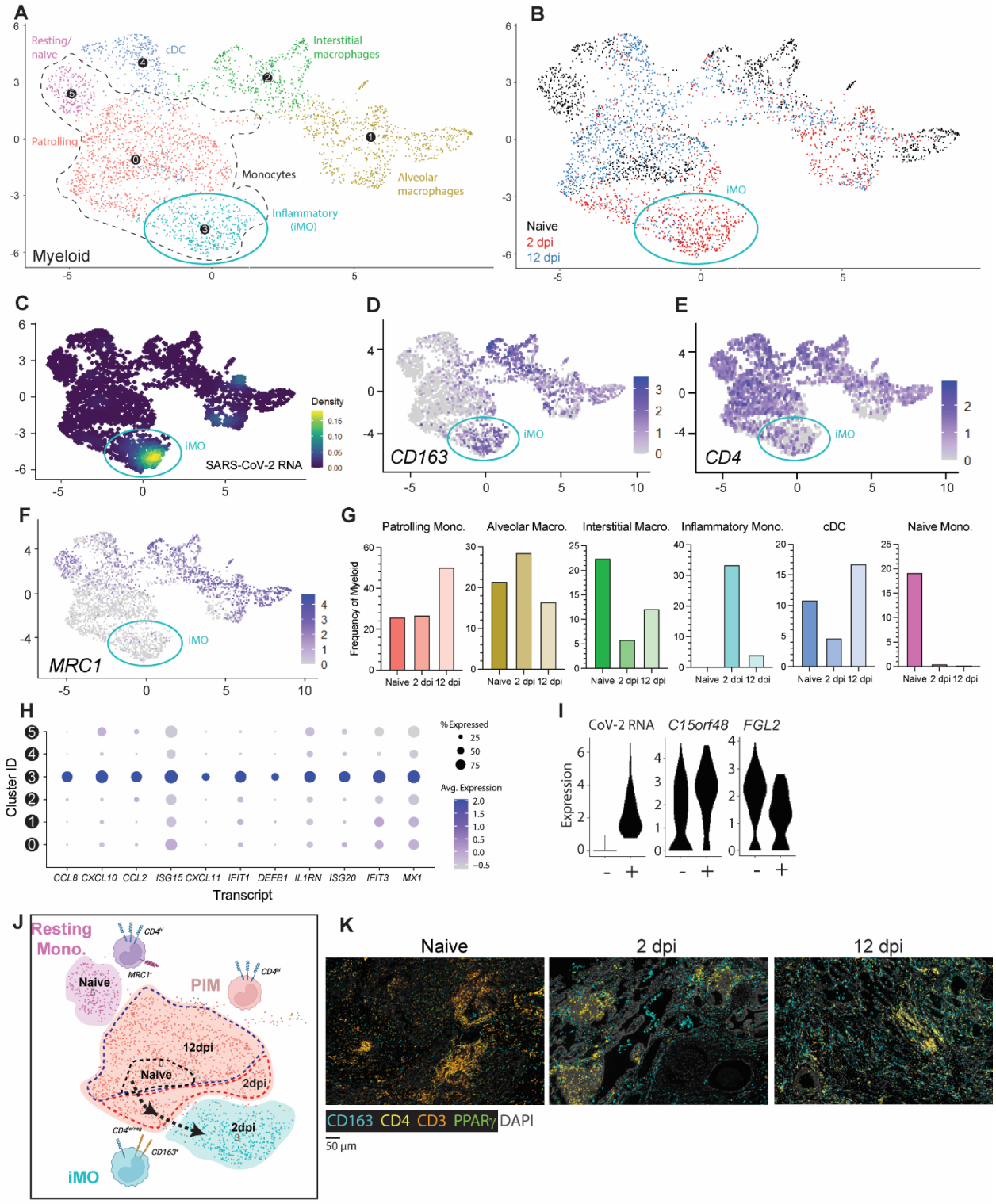

884

885

886 **Figure 4. CD163+ extravascular inflammatory monocytes arise during acute viral infection**
887 **and are predominant antiviral mediators. (A)** UMAP plot showing sub-clustering of the human
888 myeloid compartment of fLX across all time points. **(B)** Temporal annotation of the myeloid sub-
889 clusters on the UMAP plot: naïve (black), 2 dpi (red), 12 dpi (blue). ExiMO sub-cluster is indicated
890 with a blue circle. **(C)** UMAP plot (all time points) showing the distribution of SARS-CoV-2 viral
891 RNA transcripts in the myeloid compartment. **(D-F)** UMAP plot showing the expression of CD*163*
892 **(D),** *CD4* **(E)**, and *MRC1* **(F)** across myeloid sub-sets. **(G)** Frequency of each myeloid sub-cluster
893 by timepoint. **(H)** Relative expression of highly upregulated ISGs and inflammatory markers in
894 each of the myeloid sub-clusters. **(I)** Violin plots showing expression level of differentially
895 expressed genes between SARS-CoV-2 positive and negative ExiMO (sub-cluster 3). **(J)**
896 Schematic representation of proposed temporal myeloid dynamics during infection. Black arrows
897 represent differentiation dynamics during infection. **(K)** Multiplex fluorescent
898 immunohistochemistry of naïve fLX and fLX at 2 and 12 dpi. CD163: teal, CD4: yellow, CD3:
899 orange, PPARγ: green, Dapi: gray. Two representative images. Scale bar = 100 μM.
900
901
902
903
904
905
906
907
908
909

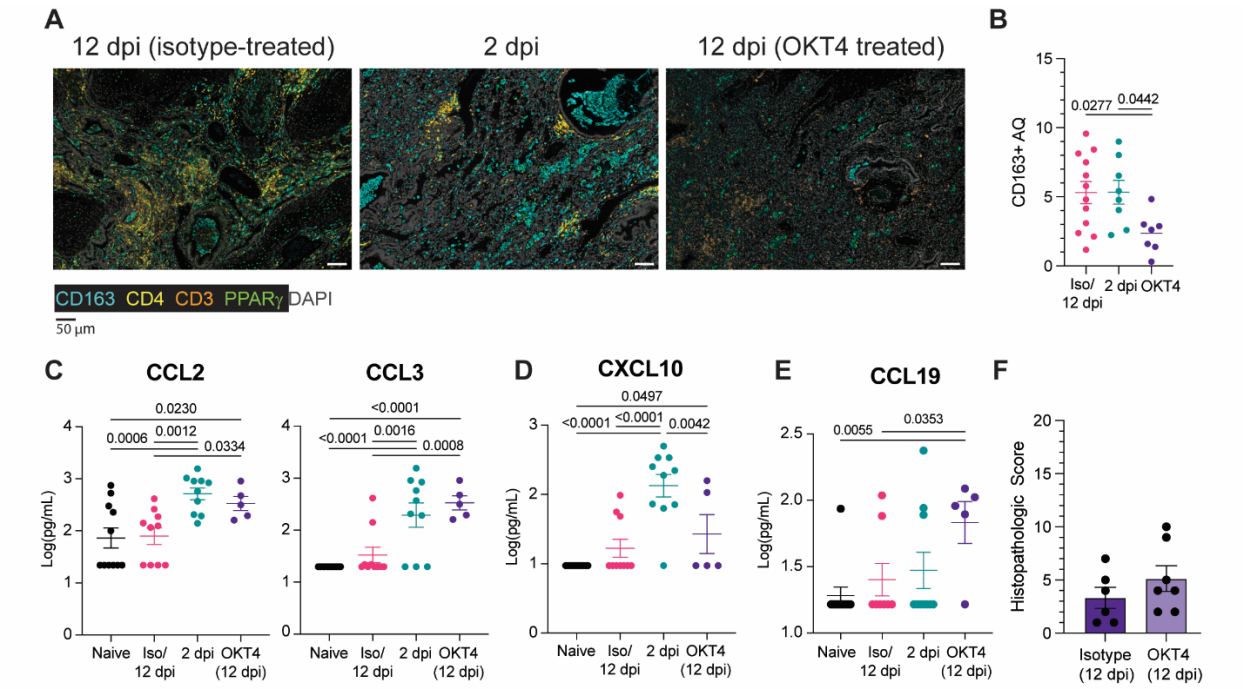

910

911 **Figure 5. CD4+ cell depletion reduces CD163+ recruitment in fLX, promotes immune**
912 **tolerance and results in signatures of chronic infection. (A-B)** Multiplex fluorescent
913 immunohistochemistry (A) and CD163+ area quantification (AQ) (B) of fLX that resolved infection
914 (12 dpi, isotype treated), or eliciting acute (2 dpi) or persistent infection (12 dpi, OKT4 treated).
915 CD163: teal, CD4: yellow, CD3: orange, PPARγ: green, Dapi: gray. Scale bar = 50 μM. **(C-E)**
916 Cytokine quantification (C: CCL2/3, D: CXCL10, E: CCL19) in the serum of naïve, infected (2 dpi
917 and 12 dpi isotype-treated or not) and OKT4-treated BLT-L mice (12 dpi). **(F)** Histopathological
918 scoring of fLX extracted from isotype and OKT4-depleted BLT-L mice (12 dpi). Error bars indicate
919 mean ± Standard error of the mean. One-*way ANOVA, t-test. p-values are indicated on graphs.*

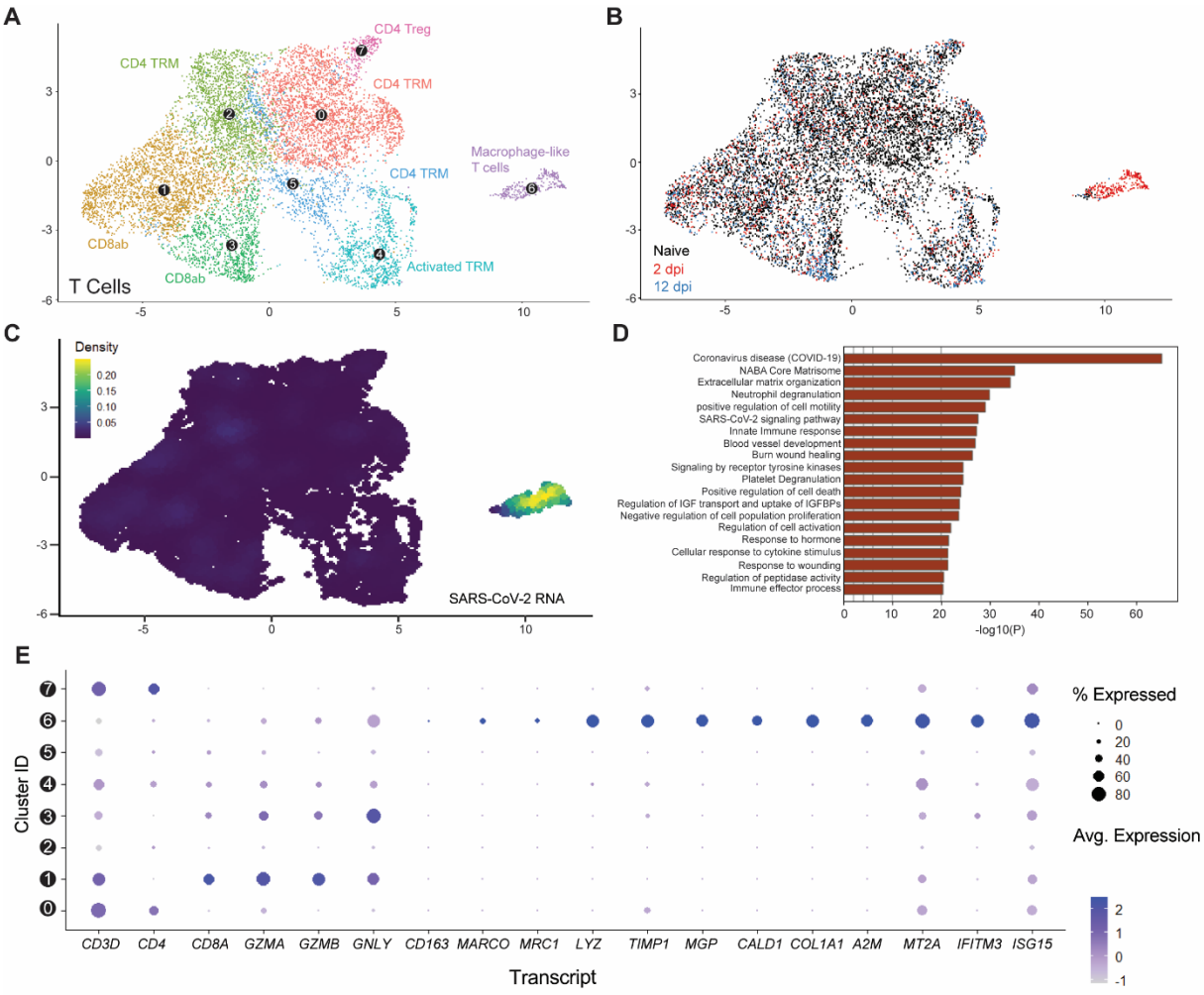

Figure 6. Macrophage-like T-cell emerges upon acute infection and are enriched in viral RNA. (A) UMAP plot showing the sub-clustering of the human T-cell compartment of fLX across all time points. **(B)** Temporal annotation of the human T-cell sub-clusters on the UMAP plot: naïve (black), 2 dpi (red), 12 dpi (blue). **(C)** UMAP plot (all time points) showing the distribution of SARS-CoV-2 viral RNA transcripts in the T-cell compartment. **(D)** Go-term analysis showing the most highly upregulated signaling pathways in the macrophage-like T-cell sub-cluster (sub-cluster 6). **(E)** Relative expression of T-cells, macrophage, mesenchymal and antiviral markers within each of the T-cell sub-clusters (From 0 to 7; as labeled in panel A.).

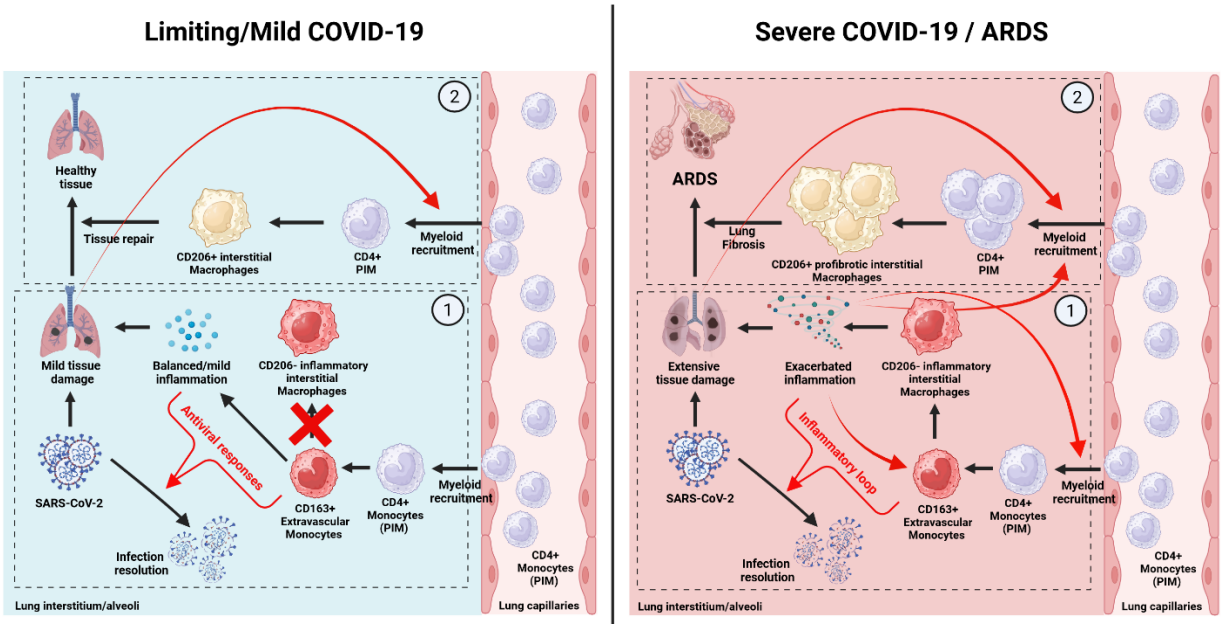

Figure 7. The inflammatory fate of ExiMO may define the clinical course of SARS-CoV-2 infection. During mild COVID-19 disease (left window), robust ExiMO antiviral responses and phagocytosis drive infection resolution in the absence of differentiation into CD206- inflammatory interstitial macrophages (1). Mild tissue damage caused by virally-induced cytopathic effects and moderate inflammation drive the recruitment of CD206+ interstitial macrophages, which promote tissue repair (2). During severe COVID-19 disease (right window), ExiMO differentiate into CD206- inflammatory interstitial macrophages. Antiviral responses and inflammation are exacerbated, triggering an inflammatory positive-feedback loop resolving infection at the expense of severe tissue damage (1). Such damages promote the extensive recruitment of CD206+ interstitial macrophages with pro-fibrotic functions, favoring the development of lung fibrosis and increasing the incidence of ARDS (2).

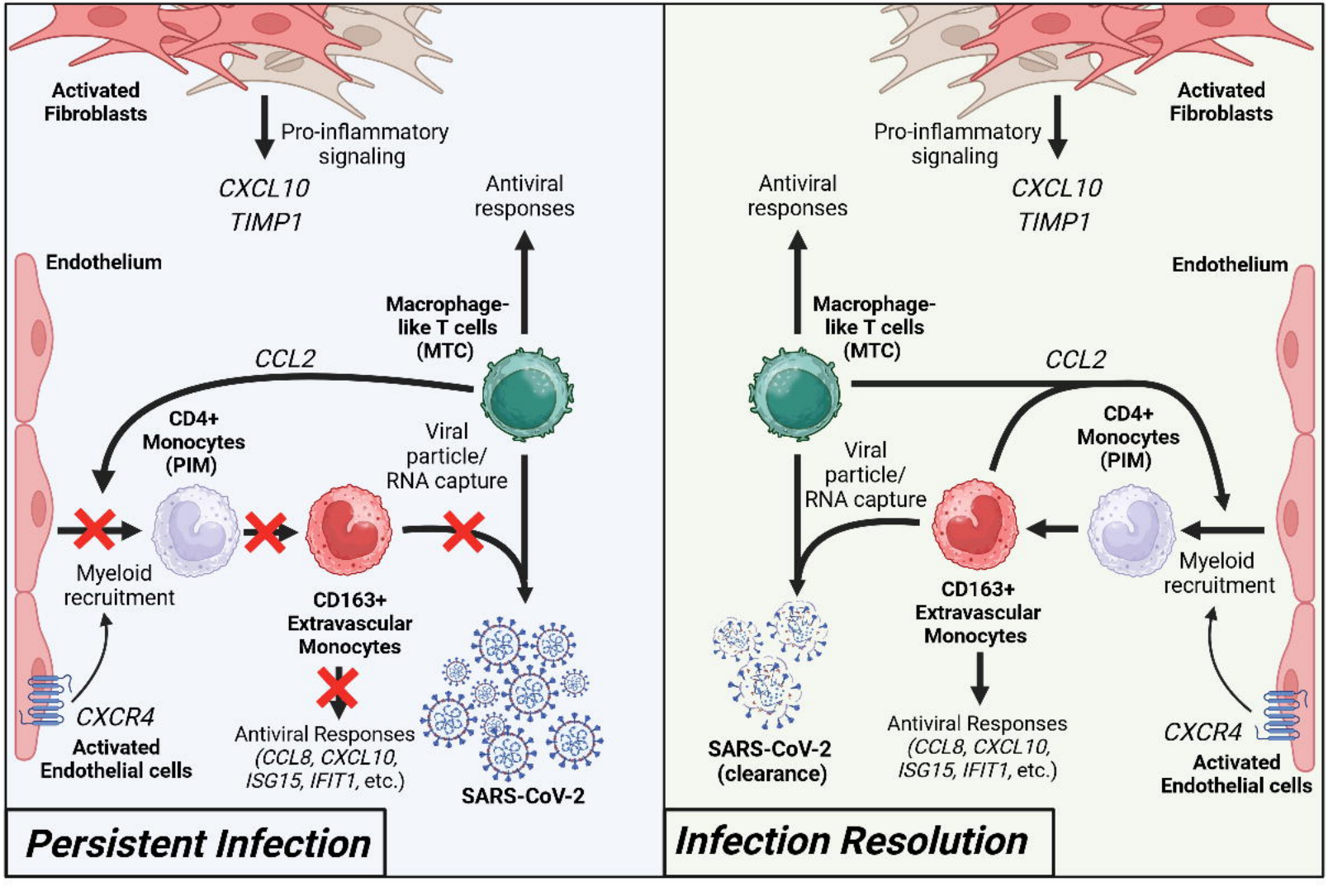
Activated Fibroblasts
Pro-inflammatory signaling
CXCL10
TIMP1
Antiviral responses
Endothelium
Macrophage-like T cells (MTC)
CCL2
CD4+ Monocytes (PIM)
Viral particle/ RNA capture
Myeloid recruitment
CD163+ Extravascular Monocytes
CXCR4
Activated Endothelial cells
Antiviral Responses (CCL8, CXCL10, ISG15, IFIT1, etc.)
SARS-CoV-2
Persistent Infection
Activated Fibroblasts
Pro-inflammatory signaling
CXCL10
TIMP1
Antiviral responses
Endothelium
Macrophage-like T cells (MTC)
CCL2
CD4+ Monocytes (PIM)
Viral particle/ RNA capture
Myeloid recruitment
CD163+ Extravascular Monocytes
SARS-CoV-2 (clearance)
Antiviral Responses (CCL8, CXCL10, ISG15, IFIT1, etc.)
CXCR4
Activated Endothelial cells
Infection Resolution